Available online at www.sciencedirect.com
ScienceDirect
Journal of the European Ceramic Society 27 (2007) 2407–2414
www.elsevier.com/locate/jeurceramsoc

A technique for measuring stresses in small spatial regions using cube-corner indentation: Application to tempered glass plates

Rajan Tandon *

Materials Reliability Department, Materials Science and Engineering Division, Sandia National Laboratories, Albuquerque, NM 87185, United States

Received 23 August 2006; accepted 10 September 2006
Available online 7 November 2006

Abstract

Vickers indentation cracks have been used to estimate residual stress in materials; however, a high threshold load for cracking limits the smallest spatial region for stress measurement. Cube-corner indenters have a lower included angle, and their sharpness leads to lowered cracking thresholds enabling stress measurement in small spatial regions. Cube-corner indentations on tempered glass plate and on annealed soda-lime-silica glass revealed that crack surface traces on the tempered material were significantly smaller. Cracks were found to be quarter-penny shaped as opposed to half-penny/radial for Vickers indentation. Using an appropriate stress-intensity factor and a stress-intensity factor superposition approach, surface stresses in the tempered plate were calculated. The stresses were in good agreement with those determined using well-established Vickers indentation approach; however, the spatial region sampled is 6–10 times smaller. An estimate of the smallest spatial region at which a particular stress may be measured using this technique is presented.

Keywords: Mechanical properties; Fracture; Hardness; Glass; Structural application; Residual stress

1. Introduction

Residual stresses are often present in ceramics and glasses at the macro-scale, either by design, as in tempered or chemically-strengthened glass,[1] or due to mismatches in elastic and thermal properties between dissimilar materials that are bonded together in engineering components as in glass-to-metal seals.[2] Adequate characterization of the stress state is an essential first step in understanding the response of the material or component to service stresses, and in assessing the reliability. Residual stress measurements therefore play an important role in design and proto-typing stages. They are also used to aid in "virtual" manufacturing. In virtual manufacturing, the entire processing sequence is simulated, and stresses during manufacture are computed using finite-element analysis (FEA). These simulations require inputs of constitutive materials models (elastic and/or visco-elastic for glasses and ceramics, elastic–plastic for metals, and visco-elastic for polymers) and thermal history of the process. There is often uncertainty in the values of these inputs, and there could be a large sensitivity of the results of the analysis to the input parameters. The fidelity of the inputs can be assessed, and material model(s) in need of refinement can be identified using residual stress measurements. Currently, for engineering design using brittle materials at Sandia, the minimum finite element mesh size ranges from 50 to 125 μm (reducing the mesh size below these values leads to unwieldy models which are cost prohibitive to run). Since cracks and defects causing failure in glasses and ceramics are typically <50 μm, it would be ideal if techniques that could sample stresses in this range are available. With the increasing importance of MEMS and MOEMS (micro-electromechanical and micro-optoelectronic devices), stress characterization in small volumes has acquired even more importance.

Residual stress measurement techniques utilized for ceramics and glasses include: birefringence methods,[3] sequential material removal and curvature measurements,[4–6] Raman spectroscopy,[7] sharp,[8–12] and blunt[13,14] indentation based techniques. Each of these techniques has its strengths and limitations: destructive (sequential material removal, indentation) versus non-destructive (birefringence, Raman), presence versus absence of specific material response (as in Raman), need for expensive

* Correspondence address: P.O. Box 5800, MS 0889, United States. Tel.: +1 505 844 1187; fax: +1 505 844 4816.
E-mail address: RTandon@sandia.gov.

0955-2219/$ – see front matter © 2006 Elsevier Ltd. All rights reserved.
doi:10.1016/j.jeurceramsoc.2006.09.001

equipment (as in Raman) versus ease of use (indentation). Often in engineering practice more than one is employed to increase the confidence in the estimates.

The indentation techniques mentioned above[8–14] have employed either a sharp Vickers indenter or a blunt spherical indenter. The use of these techniques has an inherent size limitation: the stress sampled is on the length scale of the characteristic crack size, c, emanating from the indentation site. Decreasing the load leads to a smaller hardness impression and crack size, and results in a smaller volume being sampled; however, below a certain threshold load, cracks are not observed. This issue is further exacerbated in cases where a compressive stress is to be estimated, since compression leads to an increase in the threshold load for cracking. An approach to overcoming the threshold load imposed length scale limitation has been the use of a cube-corner indenter.[15,16] The cube-corner indenter displaces approximately three times the volume of a Vickers or Berkovich indenter at the same projected contact area.[17] One consequence of higher displaced volume is that the indentation cracking threshold load is significantly reduced. For comparison, whereas a load of ~1 N is needed to initiate fracture in glass using a Vickers indentation tip, a load of only 0.005 N initiates cracking using a cube-corner tip.[15–17] In situ experiments reported in Ref.[17] show that cracking initiates almost instantaneously upon loading in glass, indicating that the threshold load is ~0 N. Kese and Rowcliffe (K–R)[18] have proposed that the lowered threshold of cracking could be used to measure residual stresses in small volumes. They related the difference in crack length in a stressed and unstressed region to the stress state. K–R utilized the technique to sample the stress in small volumes around a Vickers macro-indent in soda-lime glass. The length of cracks emanating from cube-corner indents was indeed found to be sensitive to the spatially varying stress field around the indent. However, the values of the stress calculated using the proposed formulations overestimated the stress, in some cases by a factor of 2.

The aim of this study is to further develop this promising technique by applying it to estimate the near-surface stress in a model material. Tempered glass is chosen as the model because it finds wide use in architectural and automobile windows. Additionally, previous work on stress measurements[6,8] provides a range of values for comparison to those obtained here. We report cube-corner and Vickers indentation crack length measurement results on a commercially tempered soda-lime-silica plate, and compare it to annealed (as a baseline) samples. Fractographic evidence reveals that cracks under the cube-corner indentation are "quadrant" or quarter-penny shaped, and not half-penny as was previously[18] assumed. A general stress-intensity factor superposition approach for relevant crack geometry (half-penny for Vickers and quadrant for cube-corner) is then used to estimate the surface stress. The values of compressive stress using the two approaches are similar. It is shown, therefore, that on properly accounting for the crack geometry, cube-corner indentation crack lengths can provide a good estimate of stress with the distinction that stresses are sampled over much smaller volumes. The smallest length (or volume) scale over which a particular stress is measurable for glasses is also estimated.

2. Experimental approach

A commercial soda-lime-silica glass plate, 6 mm thick (thickness denoted by h), and 508 mm × 305 mm, was obtained[i] in the fully tempered (FT) conditions. In the tempering process, glass sheets are cooled rapidly through the glass transition range. The outer region becomes rigid almost instantaneously but the low viscosity of the core prevents stress build-up. As the more fluid core cools and contracts, it is constrained by the rigid exterior, creating tension in the core and compression in the surface layers. The stress profile is approximately parabolic, with compression extending from the surfaces to ~0.27h on either side, with compensating tension in the central region.[1,6] Annealed glass (AN) of nominally the same composition was also obtained, and used as baseline.

Preliminary indentation experiments with a cube-corner indenter revealed that at loads in excess of 1.98 N, extensive lateral cracking and chipping occurred in both AN and FT materials. Since this was the lowest possible load using a conventional hardness indenter, a low load attachment[ii] was used to apply loads down to ~1 N. Indentation experiments were performed in air (relative humidity, RH = 16%) using loads 1.96, 1.47, and 0.98 N. More than 20 indentations were performed at each load. The surface traces of the three cracks from each impression, and the altitude of the surface projection of the equilateral triangle shaped hardness impression were measured optically within 5–10 min of the indentation experiments. Based on previous work[17] and our observations, it is clear that there is no measurable post-indentation growth of the cracks, and hence this time period is not critical. In some instances, extensive lateral cracking and chipping occurred even at these low loads, and those particular impression and crack sizes were not included in the data reported. However, indentations with minor lateral cracking were included. Vickers indentations in a higher load range, 9.8–107.8 N, were performed on FT plate and AN reference in air (RH = 16%), and crack lengths and impression sizes were measured immediately after indentation.

Discs, h = 3.75 mm and diameter = 38 mm, in the FT and AN conditions were also obtained from another manufacturer.[iii] Since the disc thickness is lower than the plate, identical full-temper treatments may not be as effective in generating surface stress. Cube-corner indentations at 0.98 and 1.96 N load were made on one side, and the discs were fractured in a biaxial ring-on-ring flexure set-up (loading rate = 2 MPa/s), with the indented side in tension. All the fracture surfaces were examined optically and in a FE-SEM[iv] after coating with Au–Pd thin film. These observations were used to determine the crack morphology under the indentation impression, and the mode of crack propagation to failure.

[i] PPG Industries, Pittsburgh, PA 15272, USA.
[ii] Zwick USA LP, Kennesaw, GA 30152, USA.
[iii] Swift Glass Co., Inc., Elmira Heights, NY 14903, USA.
[iv] Zeiss Supra™ SS VP, Carl Zeiss SMT Inc., NY 10594, USA.

3. Analysis

Although the stress state in tempered glass is usually approximated as parabolic with a peak compressive stress σ_s at the surface,[1,6] it can be shown[19] that the stress-intensity factor ($K = K_{HP}$) due to the residual stress, at the *surface trace* of a semi-circular (half-penny) crack is very well approximated by

$$K_{HP} = -2 f_{HP} |\sigma_s| \left(\frac{c}{\pi}\right)^{1/2} \quad (1)$$

i.e., the crack can be effectively treated as if it were loaded by a uniform compressive stress, σ_s, with the convention that compressive stresses are negative. Here, f_{HP} is a surface correction factor dependent on crack geometry and geometry of the plate.[20] Its value was assumed to be unity ($f_{HP} = 1$) in Ref.[8] for half-penny cracks. Fractographic analysis under cube-corner indentations (described in Section 4) revealed that cracks were quadrant shaped, and for this crack geometry an appropriate stress-intensity factor, K_{QP}, under a uniform load is[21]

$$K_{QP} = -F_0 |\sigma_s| \left(\frac{\pi c}{Q}\right)^{1/2} = -2 f_{QP} |\sigma_s| \left(\frac{c}{\pi}\right)^{1/2} \quad (2)$$

Here, K_{QP} is written first in the form provided in Ref.[21] Q and F_0 are factors dependent on the eccentricity of the crack, and on the eccentricity and plate thickness, respectively. Assuming that the crack is quarter-penny, i.e., eccentricity = 0, and that the crack depth is small compared to plate thickness, the expression for K_{QP} can be expressed in a form similar to Eq. (1), with the constant $f_{QP} = 1.13$. Fig. 1(a and b) shows a schematic of a half-penny crack expected under a Vickers indenter and a quarter-penny crack observed under a cube-corner indenter.

The stress-intensity factor for a half-penny crack, c_0, assumed to be point-loaded (point load = indentation load, P) at a Vickers indentation site, for an unstressed material, is given by[22]

$$K_{Ind} = \chi \frac{P}{c_0^{3/2}} = \varepsilon_{r,v} \left(\frac{E}{H}\right)^{1/2} \frac{P}{c_0^{3/2}} = K_{1c} \quad (3)$$

with $K_{Ind} = K_{1c}$ (where K_{1c} is the fracture toughness) being the equilibrium condition in an "inert" environment. c_0 is the crack length on a stress-free surface, χ, is a elastic–plastic mismatch factor, E and H are the elastic modulus and hardness, respectively, and $\varepsilon_{r,v}$ is a constant determined by indentation geometry. $\varepsilon_{r,v}$ for a Vickers indenter ranges from 0.016 to 0.022.[22,17] The stress-intensity factor for a crack around a cube-corner indenter has also been described using Eq. (3), with $\varepsilon_{r,v}$ replaced by $\varepsilon_{r,c}$. The values of $\varepsilon_{r,c}$ range from ~0.032 to 0.04.[15–18] Although there was no explicit recognition of the quarter-penny crack geometry in Refs.[15–18] (in fact Ref.[18] considers the geometry to be semi-elliptical), it must be borne in mind that $\varepsilon_{r,c}$ is a calibration that links measured crack lengths over a range of loads to the known fracture toughness. Hence the calibrations automatically include corrections due to crack geometry. This will be our rationale for using Eq. (3) for describing the indentation stress-intensity factor at a cube-corner site as well.

Therefore, for both Vickers and cube-corner indentation cracks on a stressed glass surface, the net stress-intensity factor for the measurable surface trace can be written following Ref.,[8] by combining Eqs. (1)–(3), as:

$$K_{Net} = \chi \frac{P}{c^{3/2}} - 2 f |\sigma_s| \left(\frac{c}{\pi}\right)^{1/2} \quad (4)$$

where $f = f_{HP}$ or f_{QP} as appropriate. Also noting that the equilibrium condition is $K_{Net} = K_{1c}$, and using Eq. (3) we obtain,

$$\frac{P}{c^{3/2}} = \frac{P}{c_0^{3/2}} + \frac{2 f |\sigma_s| (c/\pi)^{1/2}}{\chi} \quad (5)$$

Hence the slope of a plot of $P/c^{3/2}$ as a function of $c^{1/2}$ with an intercept fit to the value of $P/c_0^{3/2}$ allows the estimation of σ_s.

4. Results

The average cube-corner indent crack length, c_c, as a function of load for more than 20 cube-corner indentation tests on

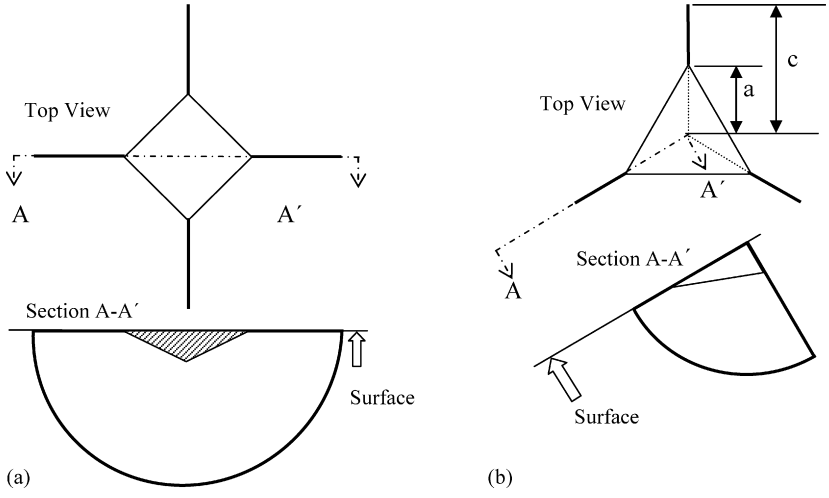

Fig. 1. (a) Schematic of a Vickers indentation site. The section view shows a semi-circular crack below the impression; (b) schematic of a cube-corner indentation site, with a section view showing the quarter-penny crack geometry. Three such cracks occur at each cube-corner site. The parameters a and c are marked. In both (a) and (b), the hatched region is the zone of plastically deformed material.

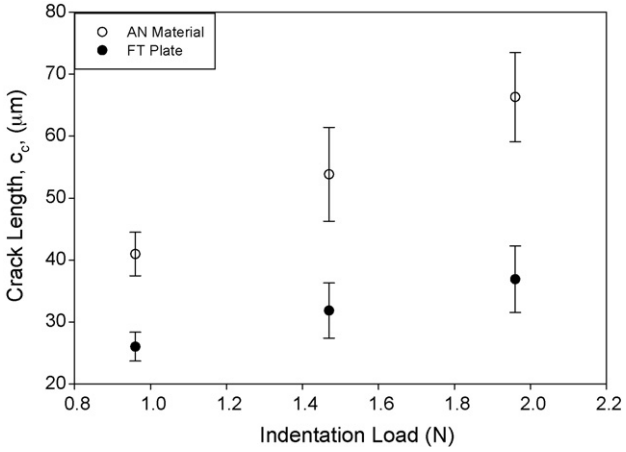

Fig. 2. Crack length as a function of load for AN and FT plate for cube-corner indentation. Results are average of 20 measurements at each of the three loads. The error bars show 1S.D. in the crack length.

AN and FT materials, measured at the three loads tested, is plotted in Fig. 2. The scatter bars represent 1S.D. in the measured crack length. At any given load, the crack lengths measured on the AN surface are significantly higher (between 55 and 80%) than those on the FT surface. The coefficient of variation, COV (COV = standard deviation/mean) of crack lengths on the FT surface is between 9 and 14%, whereas it ranges from 3 to 7% for AN material. The COV increases with load for both AN and FT materials.

The indentation parameter for cube-corner indentation, $P/c_c^{3/2}$, as function of $c_c^{1/2}$ for AN and FT materials is plotted in Fig. 3(a). The vertical and horizontal scatter bars show 1S.D. for the two quantities. The value of the indentation parameter for AN material is almost constant with increasing crack length (or increasing indentation load), with an average value of 3.78 MPa m$^{1/2}$. This value was multiplied by the uppermost value of $\varepsilon_{r,c} \sim 0.040$ reported previously,[17] and known values of $(E/H)^{1/2} \sim 3.16$ ($E = 70$ GPa, $H = 6.6$ GPa) for this material. This calibration yielded a numerical value of 0.47 MPa m$^{1/2}$, which is much less than the known fracture toughness, $K_{1c} \sim 0.7$ MPa m$^{1/2}$ for this glass. A value of $\varepsilon_{r,c} \sim 0.058$ was found to be a better calibration, and will be used in subsequent calculations. Per Eq. (4), a straight line fit for the indentation parameter such that the intercept is $P/c_0^{3/2}$ (here $c_{c,0}$ is the crack length on the AN = stress-free surface), is shown for the FT material. The slope of the line was calculated using linear regression and is marked. This slope is proportional to the value of the compressive stress, and was used to calculate the stress via Eq. (5).

Fig. 3(b) shows the $(c/2a)_c$ values for AN and FT materials as a function of load for cube-corner indents, with the scatter bars representing 1S.D. For Vickers indentation, the $c/2a$ values >1 are regarded as a sufficient condition to consider the indentation crack point loaded.[8] Assuming that similar load distribution considerations are valid for cube-corner indentation, we see that the $(c/2a)_c$ ratio well exceeds unity for the AN material, but is only slightly >1 for the FT material. Hence the assumption of point-loading due to the elastic–plastic mismatched region is likely to be valid, albeit marginally for FT material.

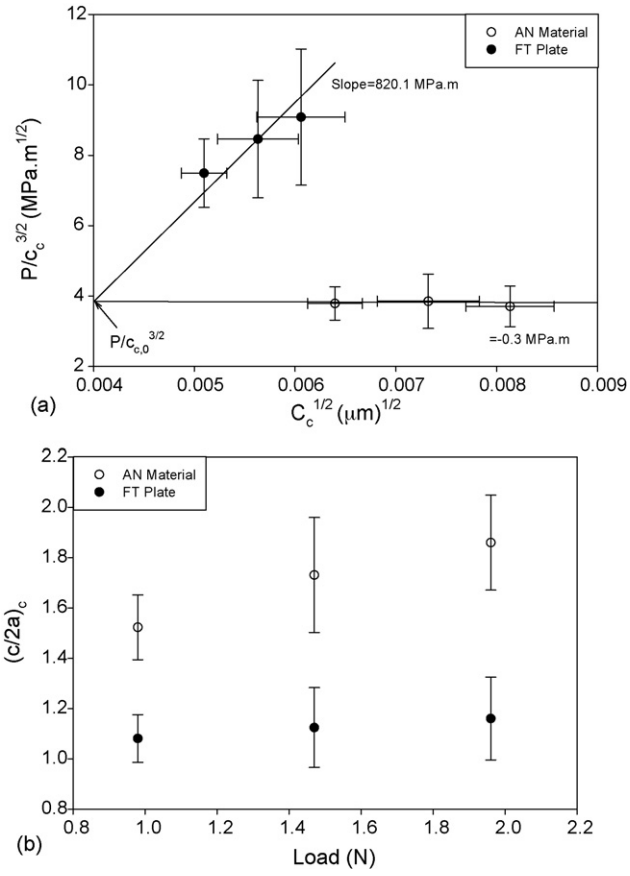

Fig. 3. (a) Plot of $P/c_c^{3/2}$ as a function of $c_c^{1/2}$ for AN and FT materials for cube-corner indentation. Best fit lines and their slopes per the relationships obtained in this work are also shown. (b) $(c/2a)_c$ ratio as a function of the load for AN and FT materials. The error bars in both (a) and (b) are 1S.D. in the measured and calculated quantities.

The indentation parameter for Vickers indentation ($P/c_v^{3/2}$) as function of $c_v^{1/2}$ for AN and FT materials is plotted in Fig. 4(a). The vertical and horizontal scatter bars show 1S.D. for the two quantities. The average $P/c_{v,0}^{3/2}$ value for AN material is 14.41, and the value of the calibration $\chi \sim 0.049$ yields the fracture toughness of 0.7 MPa m$^{1/2}$. Analogous to curve-fits in Fig. 3(a), a linear regression fit for the indentation parameter with an intercept of $P/c_{v,0}^{3/2} (= 14.41$ MPa m$^{1/2})$ is also shown. The slope of the curve fit is also included. Fig. 4(b) is a plot of the $(c/2a)_v$ ratio for Vickers indentation on the AN and FT materials. The $(c/2a)_v$ ratio exceeds unity for the AN material; however, it is less than 1 for the FT material, approaching unity only for large loads. Therefore, for the FT material, the assumption that the crack is point loaded may be questionable. However, in the absence of an alternative formulation, we will use Eq. (3) to analyze our results.

The surface stress (σ_s) calculated from the slopes shown in Figs. 3(a) and 4(a), and using $f_{HP} = 1$, for Vickers[8] was −84 MPa, and using $f_{QP} = 1.13$ [this work] for cube-corner experiments was −118 MPa. For comparison, the surface stress in tempered glass using Vickers indentation analysis[8] was estimated to be

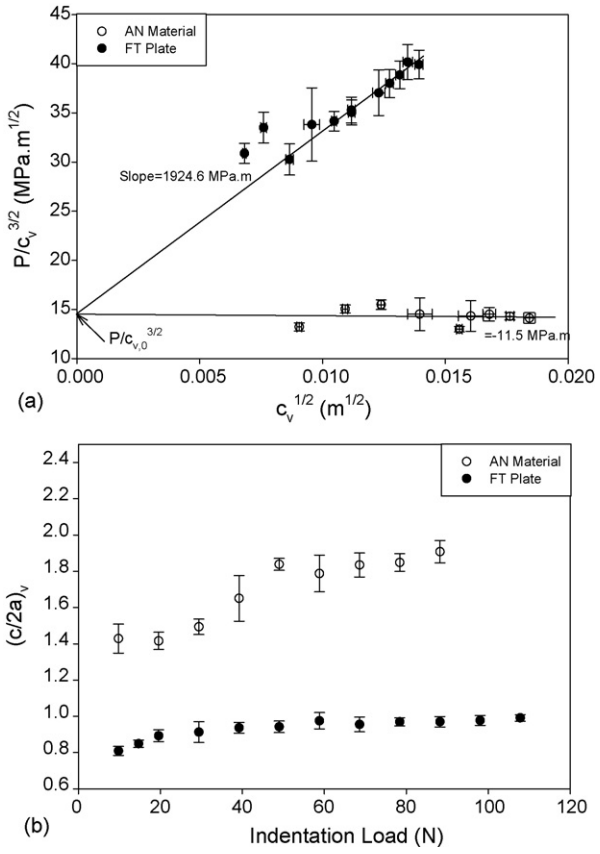

Fig. 4. (a) Plot of $P/c_v^{3/2}$ as a function of $c_v^{1/2}$ for AN and FT materials for Vickers indentation. Best fit lines and their slopes per the relationships obtained in this work are also shown. (b) $(c/2a)_v$ ratio as a function of the load for the two materials. The error bars in both (a) and (b) are 1S.D. in the measured and calculated quantities.

−130 MPa. The discrepancy between the values (both obtained from Vickers indentation data) could be due to the fact that $(c/2a)_v$ was <1 in our material, whereas this value was reported to be >1 for higher loads in Ref.[8] This point will be discussed in the next section. However, the values obtained in our study using cube-corner and the Vickers results in Ref.[8] are in the same range, indicating that our approach is viable.

The AN and FT disks with 0.98 and 1.96 N load cube-corner indents were fractured in biaxial loading at 2 MPa/s loading rates, and the fracture surfaces were examined in FE-SEM. Fig. 5(a) shows the results for AN material that fractured from 0.98 N load indent. The as-indented crack length on the top surface is marked. The images show that *two* cracks, emanating from two vertices of the hardness impression, propagate to cause failure. More importantly, it can be observed that the shape of the crack is not half-penny or radial, but "quadrant"; i.e., the cracks observed on the free-surface are quarter-circles (or ellipses) below the surface, intersecting each other below the central point of the hardness impression. One of these quadrant cracks is delineated using dotted lines. Upon biaxial loading, these cracks propagate in their respective planes to cause failure. Twist hackle features, which normally indicate a change in the stress state acting on a crack, are visible at the crack boundary, and are indicative of the location where unstable crack propaga-

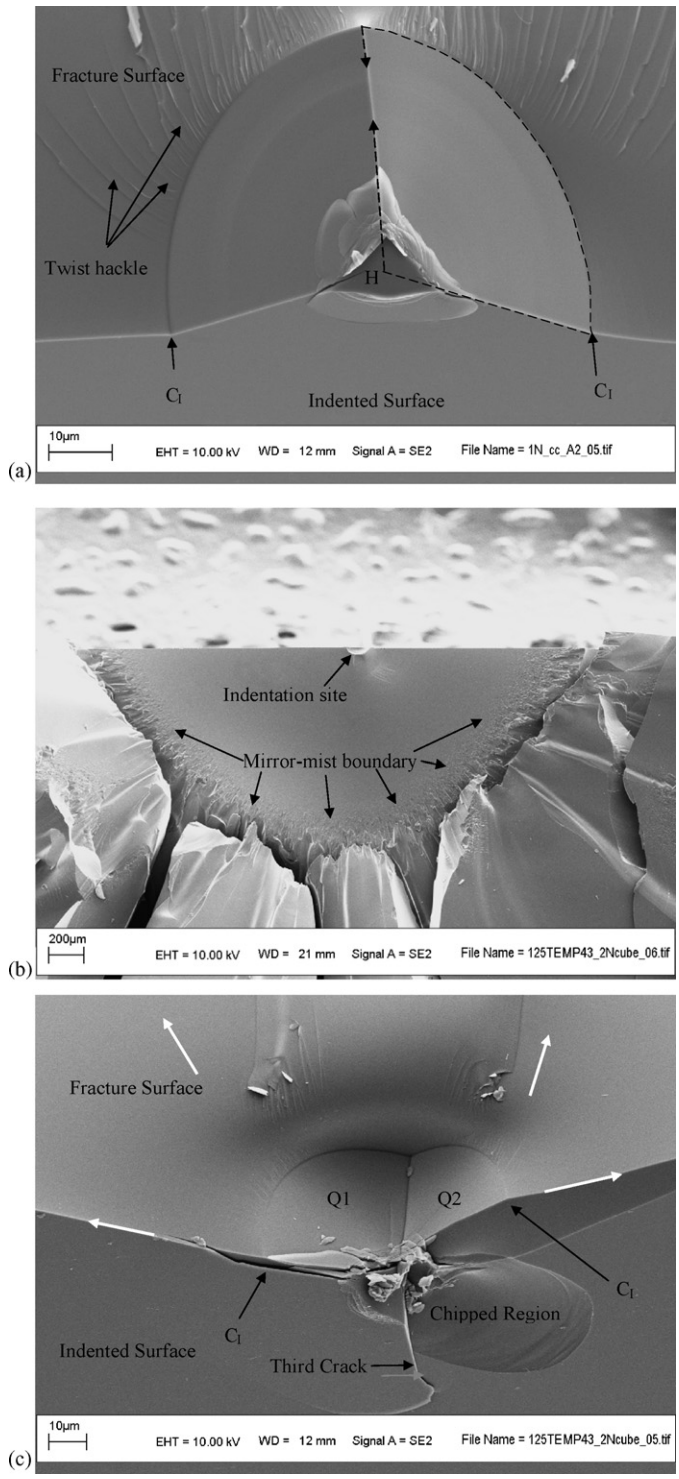

Fig. 5. Fracture surfaces of disks tested in biaxial tension after cube-corner indentation at (a) 0.98 N load on AN. The as-indented crack length on the top surface (C_I), and the hardness impression (H) are marked. One of the quadrant cracks is delineated by the dotted lines. Twist hackle features are visible. (b) View of 1.96 N load fracture site on FT material. The indentation site and mirror-mist boundary is marked. (c) Close-up view of 1.96 N load fracture site in (b). The two quarter-penny cracks, Q1 and Q2, are indicated. The third crack that did not participate in the fracture process, and a chipped region due to lateral cracking are shown. The white arrows indicate the direction of crack propagation.

tion started. The FT material has high stored elastic strain energy due to the tempering stresses. When 0.98 N load indents were the origins of fracture, the combination of the high applied stress and the residual stress led to extensive fragmentation. Therefore, fracture surface images for this load could not be obtained; however, fracture surfaces views for the 1.96 N load failure are shown in Fig. 5(b and c). Fig. 5(b) is a low magnification image that has the indentation site marked. The mirror-mist boundary is indicated. Fig. 5(c) is a higher magnification image of the indentation site. The two original quadrant cracks, Q1 and Q2, are marked. The ends of the surface traces of these cracks are indicated as C_I. The white arrows show the direction of crack propagation to failure. The third crack (on the free surface) that did not participate in the sample fracture is shown. Also marked is a lateral crack chip at the indentation site. It is clear that at least at this load, the indentation crack morphology remains quarter-penny even on a tempered surface.

5. Discussion

The data in Fig. 2 show that there is a statistically significant difference between the average crack sizes on the AN and FT materials at all three loads tested. Crack sizes ~25 μm at the lowest indentation load (0.98 N) are sufficient to experimentally resolve stresses of the magnitude found in the FT material (~−120 MPa). Hence the cube-corner indenter can easily serve as a useful surface probe to measure stresses of the order of 100 MPa in a 25^3 μm^3 volume. The indentation technique, however, has a lower length (or volume) limitation, imposed by two factors: (1) if the load falls below the cracking threshold, no cracking is observed, and this threshold load increases with an increase in the compressive stress. The use of a cube-corner indenter effectively overcomes this first factor, at least for the (relatively low) compressive stresses found here. (2) The second factor is a consequence of the K value due to the residual stress loading (both Eqs. (1) and (2)) being proportional to $c^{1/2}$. At small values of c, the $|K|$ is small; consequently, its effect on the measured crack length may be minute enough to be within the experimental scatter in crack length measurements. As the crack length increases, the $|K|$ increases for the surface stressed FT glass, and crack length become distinguishable (beyond 1S.D.) between the stressed and unstressed material. From work presented in Ref.,[19] much lower stresses in glasses (~−30 MPa) are resolvable over a ~20^3 μm^3 volume, demonstrating that cube-corner indentation is an ideal tool for measuring point-to-point residual stress variations in materials.

The data in Fig. 2 also indicate that there is a higher scatter in crack lengths, COV ~ 9–14%, for the FT surface as compared with COV of 3–7% for the AN material. The higher scatter in COV for the FT material could be due to (at least) two factors: (1) the process of inducing the residual surface stress (air-jet impingement on the surface for cooling) may lead to small regions that have different cooling rates from each other, thereby leading to a slight non-uniformity in the stress value and/or (2) the interaction of the residual stress with the stress field of the indentation leads to enhancement of the incidence and extent of lateral cracking. (Here, it must be borne in mind that although indentations that had extensive lateral cracking and chipping were excluded from measurements, surface traces of many with only limited lateral cracking were included in the measurements.) This phenomenon has been observed previously[23] on compressively stressed surfaces for Vickers indentation. Lateral cracking reduces the driving force for the half-penny cracks under a Vickers site,[24] and has, presumably, the same effect on the quarter-penny cracks under a cube-corner site. Then, the scenario for the larger variation in crack lengths would be that if lateral cracking does not occur, surface traces of cracks of a particular length with average size c_{NLC} ($c_{NLC} < c_0$) would be observed; however, with lateral cracking, an even smaller average surface trace, c_{LC} ($c_{LC} < c_{NLC}$) would be measured. For a group of indentations on a compressively stressed surface, crack length values would be distributed around both c_{LC} and c_{NLC}, leading to a large scatter in the measured data. The data also reveal that the COV increases with increasing load for both materials. Since the first factor mentioned above (residual stress variations) is absent for the AN material, this increase can be directly attributed to the greater propensity for lateral cracking with increasing load. Also, for the FT plate, at least half of COV can be attributed to enhanced lateral activity.

Now assuming that for all loads below 1 N, there is approximately a 10% COV for FT material, and a COV of 3% for AN material, a rough estimate of the spatial stress resolution capability of the cube-corner indentation technique was made as follows: using Eq. (3) and the parameter χ for cube-corner indentation ($\chi \sim 0.058 \times 3.16 = 0.183$), crack lengths ($c_0$) on AN material were calculated as a function of loads ≤1 N. The calculated values are shown as open circles in Fig. 6. The solid line is the value of the lower limit for c_0 ($=c_0 - 0.03c_0$) at 1S.D. Then, solving Eq. (5) iteratively, the crack lengths, c, and upper limit of these crack lengths at 1S.D. ($=c + 0.1c$) were calculated for assumed values of residual compressive stress (=50, 100, and 200 MPa). The crack length values are shown as open symbols,

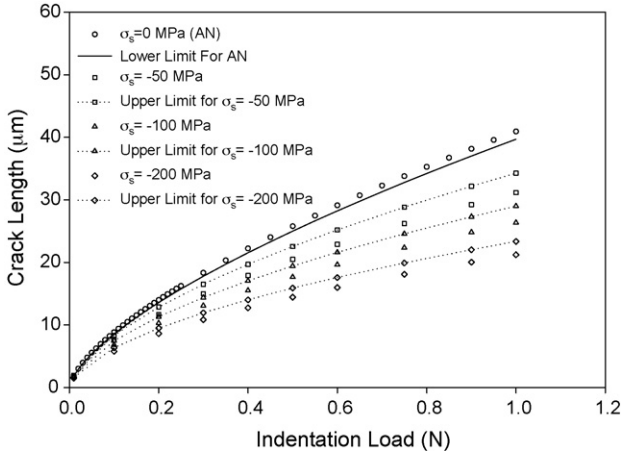

Fig. 6. Results of calculations showing the stress resolution capability of the cube-corner indentation technique. The open symbols are mean values of crack lengths as a function of load expected for surface stress values of 0, −50, −100, and −200 MPa. The solid line is lower limit (at 1S.D.) for AN material assuming a COV of 3%. The dotted lines with open symbols are the upper limit (at 1S.D.) for each of the compressive stress levels assuming a COV of 10%.

and the corresponding upper limit values are shown as open symbols with a dotted line through them. For any stress, the minimum load for which this dotted line is clearly resolvable from the solid line (for the AN material) should be located. The crack length corresponding to this minimum load is the length scale at which that particular value of stress can be measured. For example, examining Fig. 6, we conclude that for glasses a 200 MPa stress may be measured over a length of ∼5 μm (load ∼ 0.1 N), whereas a crack size of ∼15 μm (load ∼ 0.3 N) is necessary to resolve a stress of 50 MPa, i.e., higher compressive stresses can be measured over small spatial dimensions, with the proviso that the (smaller) loads employed exceed the threshold load.

A value of $\varepsilon_{r,c} \sim 0.058$, that is considerably higher than previous estimates of 0.032–0.040, was obtained. This could be the result of difference in relative humidity (RH) experienced by the crack in the two studies. Our work was conducted in relatively dry (16% RH) ambient lab air, whereas Ref.[15] does not specify humidity. Higher RH would lead to longer measured crack lengths after indentation. When these (longer) crack lengths are used to calibrate to a fixed toughness a lower value of $\varepsilon_{r,c}$ is obtained. It is interesting to note that several data points in Fig. 3, Ref.[17] for soda-lime glass lie above the line drawn using $\varepsilon_{r,c} \sim 0.04$, indicating, perhaps, that a higher value for this calibration factor may be more appropriate. There is also a possibility there are systematic differences in the loading and measurement set-ups that contribute to this difference. Knowing the absolute value of this parameter is important; however, since our calculations utilize a difference between baseline (AN) behavior and FT material to compute stress, the absolute values are not overly critical.

In the earlier K–R study,[18] cracks emanating from cube-corner indentation were described as radial (Figs. 2 and 3 in Ref.[18]). The authors, however, noted that they had experimental difficulty in inducing failure from indentation sites, and examining the fracture surface. It should also be mentioned the fracture surface image shown (Fig. 3 in Ref.[18] for a cube-corner indentation load of 0.7 N) is rather indistinct, and the crack morphology cannot be observed clearly. Observation presented in Fig. 5(a) for AN disc with fracture originating from a 0.98 N load cube-corner indent, and Fig. 5(c) for a FT material with a 1.96 N load indent, clearly show the "quadrant" crack morphology. In Fig. 5, the crack shape is delineated using dotted lines. Fig. 1(b) is a schematic top and section view of the crack geometry observed at the cube-corner indentation site in soda-lime-silica glass: three cracks whose surface traces appear to emanate from the vertices of the indentation (at 120° from each other), with a quadrant shape in the depth, extending to meet each other at the projection of the centroid of the impression.

Using the values provided by K–R, and recasting their analysis to conform to Eqs. (2) and (3), we find the value of f used by them is 0.543. Examining Eq. (5), it is clear that for the same value of measured slope, using the f from K–R analysis would lead to a stress value $\sim 1.13/0.543 = 2.08$ times higher than what we obtain (−118 MPa). Since the actual stress in the tempered glass is of the order of ∼−100 MPa, the K–R crack shape assumption would have led to an overestimate.

The Vickers indentation technique results slightly underestimate the surface stress for the FT material. It is important to note that $(c/2a)_v$ values for FT do not exceed unity (Fig. 4(b)) even at 110 N load. For such short crack lengths, the loading due to the elastic–plastic mismatched region cannot accurately be considered point-loaded, and Eq. (3) may not be precise. A rough estimate of the error in using Eq. (3) may be obtained by comparing the stress-intensity factors for an internal penny-shaped crack loaded by point force, P, and by a circular distribution of stresses (σ_p) around its center such that $\pi a^2 \sigma_p = P$.[25] It is found that for $0.8 < c/2a < 1$, the stress-intensity factor around the center-loaded crack is ∼7–12% greater than that for the point-loaded crack. Hence it is likely that for short ($c/2a < 1$) half-penny cracks, the point-loaded stress-intensity factor relation (Eq. (3)) underestimates the actual stress-intensity factor by ∼10%. Using Eq. (4), it can be shown that for the values of $P/c_v^{3/2}$ obtained in our work, this underestimate leads to an underestimate of the σ_s value of ∼20%. Details of this necessary correction, which would bring the predicted values of the Vickers indentation closer to the expected values of stress in this material, are a subject of future work.

6. Summary and conclusions

A stress-intensity factor superposition approach, based on established fracture mechanics models, was developed for cube-corner indentation. Indentation crack length data were utilized to estimate the residual stress on a commercially tempered glass plate. The crack shape under a cube-corner indentation was shown to be a quarter penny on both the stressed and unstressed glass surfaces. A stress-intensity factor relevant for this geometry was calculated, and used in a stress-intensity factor superposition approach to accurately estimate stress. Assuming that the COV's in the crack lengths stay at the levels measured at 0.98 N, a calculation was performed to estimate the stress resolution of the technique. It was found that higher compressive stresses can be measured at a finer resolution. Overall, the cube-corner indentation approach is found to be a very effective technique for measuring stresses in small spatial dimensions.

Acknowledgements

Sandia is a multi-program laboratory operated by Sandia Corporation, a Lockheed Martin Company, for the United States Department of Energy's National Nuclear Security Administration under Contract-DE-AC04-94AL85000. SEM work by Bonnie McKenzie, and measurements by Karl Nieman, both at Sandia, are gratefully acknowledged. Deidre Ragan at PPG Industries kindly supplied the glass plates used in the study.

References

1. Barsom, J. M., Fracture of tempered glass. *J. Am. Ceram. Soc.*, 1968, **51**, 75–78.
2. Varshneya, A. K. and Petti, R. J., Finite element analysis of stresses in glass-to-metal foil seals. *J. Am. Ceram. Soc.*, 1978, **61**, 498–503.

3. McKenzie, H. W. and Hand, R. J., *Basic Optical Stress Measurement in Glass*. Society of Glass Technology, Sheffield, UK, 1999, 96 pp.
4. Treuting, R. G. and Read Jr., W. T., A mechanical determination of biaxial residual stress in sheet materials. *J. Appl. Phys.*, 1951, **22**, 130–134.
5. Virkar, A. V., Determination of residual stress profile using a strain gage technique. *J. Am. Ceram. Soc.*, 1990, **73**, 2100–2102.
6. Tandon, R. and Green, D. J., Residual stress determination using strain gage measurements. *J. Am. Ceram. Soc.*, 1990, **73**, 2628–2633.
7. Tallant, D. R., Michalkse, T. A. and Smith, W. L., Effects of tensile stress on the Raman spectrum of silica glass. *J. Non-Cryst. Solids*, 1988, **106**, 380–383.
8. Marshall, D. B. and Lawn, B. R., Indentation technique for measuring stresses in tempered glass surfaces. *J. Am. Ceram. Soc.*, 1997, **60**, 86–87.
9. Lawn, B. R. and Fuller, E. R., Measurement of thin layer surface stresses by indentation fracture. *J. Mater. Sci.*, 1984, **19**, 4061–4067.
10. Gruninger, M. F., Lawn, B. R., Farabaugh, E. N. and Wachtman, J. B., Measurement of residual stresses in coatings on brittle substrates by indentation fracture. *J. Am. Ceram. Soc.*, 2003, **70**, 344–348.
11. Tandon, R. and Green, D. J., Indentation behavior of ion-exchanged glasses. *J. Am. Ceram. Soc.*, 1990, **73**, 970–977.
12. Morris, D. J., Myers, S. B. and Cook, R. F., Indentation crack initiation in ion-exchanged aluminosilicate glass. *J. Mater. Sci.*, 2004, **39**, 2399–2410.
13. Roberts, S. G., Lawrence, C. W., Bisrat, Y., Warren, P. D. and Hills, D. A., Determination of surface residual stresses in brittle materials by Hertzian indentation: theory and experiment. *J. Am. Ceram. Soc.*, 1999, **82**, 1809–1816.
14. Swadener, J. G., Taljat, B. and Pharr, G. M., Measurement of residual stress by load and depth sensing indentation with spherical indenters. *J. Mater. Res.*, 2001, **16**, 2091–2102.
15. Pharr, G. M., Harding, D. S. and Oliver, W. C., *Measurement of Fracture Toughness in Thin Films and Small Volumes Using Nano-indentation Methods. Mechanical Properties and Deformation Behavior of Materials Having Ultra-Fine Microstructures*. Kluwer Academic Publishers, Netherlands, 1993, pp. 449–461.
16. Pharr, G. M., Measurement of mechanical properties by ultra-low load indentation. *Mater. Sci. Eng. A*, 1998, **A253**, 151–159.
17. Morris, D. L. and Cook, R. F., *In situ* cube-corner indentation of soda-lime silica glass and fused silica. *J. Am. Ceram. Soc.*, 2004, **87**, 1494–1501.
18. Kese, K. and Rowcliffe, D. J., Nanoindentation method for measuring residual stress in brittle materials. *J. Am. Ceram. Soc.*, 2003, **86**, 811–816.
19. Tandon, R. and Buchheit, T. E., *J. Am. Ceram. Soc.*, in press.
20. Newman, J. C. and Raju, I. S., An empirical stress intensity factor equation for the surface crack. *Eng. Frac. Mech.*, 1981, **15**, 185–192.
21. Zheng, X. J., Glinka, G. and Dubey, R. N., Stress intensity factors and weight functions for a corner crack in a finite thickness plate. *Eng. Frac. Mech.*, 1996, **54**, 49–61.
22. Anstis, G. R., Chantikul, P., Lawn, B. R. and Marshall, D. B., A critical evaluation of indentation techniques for measuring fracture toughness: I. Direct crack measurements. *J. Am. Ceram. Soc.*, 1981, **64**, 533–538.
23. Tandon, R., Green, D. J. and Cook, R. F., Surface stress effects on indentation fracture sequences. *J. Am. Ceram. Soc.*, 1990, **73**, 2619–2627.
24. Cook, R. F. and Roach, D. H., The effect of lateral crack growth on the strength of contact flaws in brittle materials. *J. Mater. Res.*, 1986, **1**, 589–600.
25. Tada, H., Paris, P. C. and Irwin, G. I., *The Stress Analysis of Crack Handbook* (*third ed.*). ASME Press, New York, 2000.